Doubly differential measurements for multiple ionization of argon by electron impact: Comparison with positron impact and photoionization

A. C. F. Santos, A. Hasan, T. Yates, and R. D. DuBois
Department of Physics, University of Missouri–Rolla, Rolla, Missouri 65409
(Received 23 January 2003; published 27 May 2003)

Doubly differential cross sections for single and multiple ionization of Ar have been measured for 500, 750, and 1000 eV electron impact. The cross sections were measured as a function of projectile energy loss and scattering angle. The energy loss range was 0–85 % of the initial projectile energy and scattering angles were between $\pm 22°$. The data were put on an absolute scale by normalizing to total ionization cross sections available in the literature and found to be in good agreement with the absolute electron impact cross sections from DuBois and Rudd. For 750 eV impact, a comparison was made between the present electron impact data and positron impact data obtained using the same experimental conditions. The same energy dependence and yields for single ionization were found for both electron and positron impact. On the other hand, the double- and triple-ionization yields are smaller for positron impact as compared to electron impact. Comparisons with photoionization data showed that for outer shell ionization the fractions of double and triple ionization of argon by photon impact are in quite good agreement with the present electron impact data.

DOI: 10.1103/PhysRevA.67.052708 PACS number(s): 34.80.Dp, 34.85.+x

I. INTRODUCTION

At high velocities, the Born approximation predicts that the inelastic cross section depends on the square of the charge of the incoming particle, q, and on the impact velocity v as $q^2 v^{-2} \ln v^2$. Therefore, the single-ionization cross sections are expected to be the same for electrons, positrons, and protons traveling at the same speed [1]. Nevertheless, for velocities near to 10 a.u., differences between equal velocity electrons and protons have been reported for increasing target atomic number in the single-ionization cross sections [2]. Whether this is a result of changing the sign of the projectile charge, because of the vastly different projectile masses, or associated with an unknown source is uncertain.

One method of answering this question is to isolate charge effects and study them independently, as can be done by comparing particle and antiparticle impact data. For this and other reasons there has been a rapid growth in the number of studies comparing particle and antiparticle impact in recent years [3–13]. This growth can be attributed in part to advances in the availability of positron sources. From these studies, remarkable features have been observed in the total cross sections for particle and antiparticle impact. For example, Andersen *et al.* [10] measured multiple ionization of light noble gases by protons and antiprotons and found that the single ionization cross sections of He, Ne, and Ar are identical within experimental uncertainties at energies from 0.5 to 5 MeV. On the other hand, double ionization by antiprotons was found to be a factor of 2 larger than the corresponding ionization by proton impact. As pointed out by Paludan *et al.* [8,9], who measured single and double ionization by positrons and antiprotons and compared with existing electron and proton data, the negative charged particles are favored as compared to the positive ones due to the increasing static interaction between the projectile and the target nucleus. However, to date, little information concerning the dynamics associated with changing the projectile charge and mass is available.

Unfortunately, to understand these effects requires a detailed description of multiple ionization. This is far from a simple task due to the complexity of the many possible pathways leading to it and due to the presence of many bodies mutually interacting through the long-range Coulomb force. For instance, the double ionization of atoms has been interpreted in terms of either the shake-off or two-step process, but also occurs after a postcollisional Auger decay as a consequence of inner-shell ionization. Despite the fact that multiple ionization of atoms by electrons has been exhaustively studied for decades, many of its features are still rather unknown and to date comparison between differential multiple ionization cross sections for particle and antiparticle impact is nonexistent in the literature.

Another impetus for the present work is the connection between the impact of fast charged particles and photoabsorption that has long been made [1]. In fact, the perturbation experienced by the target in the interaction with the incident charged particle may be regarded as tantamount to a photon pulse, with the Fourier transform of the electric field granting the frequency components. In this sense, the projectile energy loss is equivalent to the energy of an absorbed photon. However, they may not be identical due to the fact that the ejected electron, as a rule, is slower for charged-particle impact than for high-energy photon impact [9], and the rearrangement process is strongly sensitive to final-state correlations.

To address some of these questions, we have measured double-differential multiple ionization cross sections of argon by 500, 750, and 1000 eV electron impact. Data are obtained as a function of scattered projectile energy and angle, using coincidence techniques, for energy losses ranging from 0 to 85% of the initial electron energy, and for scattering angles between $\pm 22°$. The results are compared to 750 eV positron impact data obtained using the same experimental conditions. For this comparison, the previously reported positron impact cross sections have been slightly adjusted to account for additional information regarding

detection efficiencies. In addition, the data are compared to photoionization data.

II. EXPERIMENT

The experimental setup was described elsewhere [14,15]. In brief, an electron beam produced by secondary emission from a tungsten moderator coupled to a positron source intersects a gas jet of argon emerging from a needle source. The forward-scattered projectiles are energy analyzed by an electrostatic spectrometer and recorded by a microchannel plate position sensitive detector. The spectrometer focuses electrons onto the detector, which is located at the focal plane of the analyzer. The horizontal location of the focus is dependent on the final energy E of the scattered electrons and the vertical location depends on their scattering angles.

For the present studies, the horizontal and vertical acceptance angles for scattered projectiles were $\pm 6.5°$ and $\pm 22°$, respectively. The vertical angles were calibrated by deflecting the beam with a known electric field and measuring the vertical position on the detector after the deflected beam passed through the entrance slit at a known position. The angle calibration was found to be linear in the vertical angular range $\pm 12°$. For angles between approximately 12° and 22°, all scattered projectiles arrived at roughly the same vertical position on the detector due to fringing fields and the large acceptance angle of the spectrometer. Due to the beam collimation used a finite spot size is formed on the detector, giving an angular resolution of $\pm 1°$.

To calibrate the spectrometer plus detector energy resolution, the following procedure was used. First, the injected beam energy and resolution were measured by inserting a channel plate detector in the beamline and using the retarding field method to sample the energy distribution and to establish the mean energy. It was found that our secondary emission source had an energy spread of roughly 12–15 eV (full width at half maximum). Then, using beams of known energy, the position on the detector was recorded as a function of spectrometer voltages. A linear dependence between the beam energy and the detected position was found. This linear dependence was also shown to be the same for all ''energy-loss'' ranges that could be observed for specific spectrometer voltages. Because of the diameter and energy spread of the electron beam, the large range of scattering angles accepted by the spectrometer, and lensing effects in the spectrometer, scattered electrons of a given energy focused to an extended region on the detector, rather than to a single point. Due to the above-mentioned facts, the present energy resolution is roughly 15 eV or larger. This low energy resolution introduces uncertainties near the thresholds for single and multiple ionization but does not influence their overall behaviors and relative importance as a function of projectile energy loss.

Data acquisition was as follows. Electron beams with intensities between 20 and 40 kHz and diameters of 2 mm were injected. Energy-loss spectra were recorded by placing appropriate voltages on the spectrometer plates and using the projectile detector to measure electrons scattered (or ionized) into forward angles and having a specific range of energy losses. The ionized recoil ions were extracted from the collision region by a weak electric field (10 V/cm). After passing through a high-transmission grid located at the entrance of a time-of-flight (TOF) mass spectrometer, they separated according to their mass-to-charge ratio and were detected by a microchannel plate detector biased at -2800 V. A position sensitive anode provided information about their origin. This aided in isolating ''target'' from ''background'' ionization events. The recoil ions were used to start a time-to-digital converter, which was stopped by the signals from the projectile detector. Using a time-to-digital converter and a PC, list mode data were collected. The total number of recoil ions was also used to normalize data recorded at different energy-loss ranges and to place the data on an absolute scale. Typical coincidence signal rates were of the order of 10–30 Hz or smaller depending on the energy-loss regime.

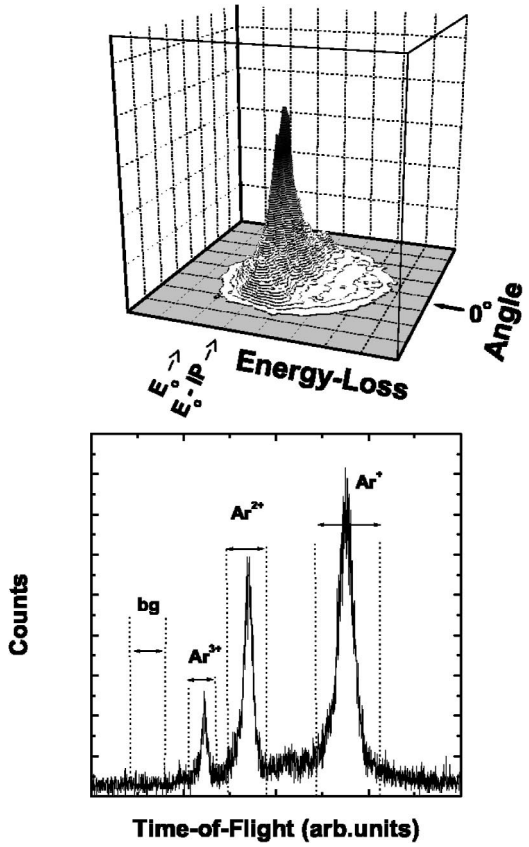

FIG. 1. Bottom: Time-of-flight spectrum of multiply charged argon ions for 1 keV electron impact in the energy-loss range from 253 to 352 eV. The vertical lines indicate the region of interest used as software restrictions with regard to sorting list-mode data. Top: 3D plot of scattered projectile electrons as a function of projectile energy loss and vertical scattering angle. Data are for 1 keV impact. E_0 indicates the position of the main beam and E_0-IP (ionization potential) the threshold for single ionization of argon.

With target gas present, the chamber pressures were $(1-2)\times 10^{-5}$ Torr and the target densities were roughly 60 times higher. For these conditions, the coincidence TOF signals yielded comfortably separated peaks for different charge states of the recoil ions, as shown in Fig. 1, plus small contributions from residual gas impurities (e.g., N_2^+, O_2^+,

H_2O^+). The areas under the peaks were integrated and corrected by the corresponding detection efficiencies [16]. After subtracting a background, also shown in Fig. 1, the peak areas provide information about the single- and multiple-ionization yields. Then, by placing software restrictions on the projectile detector positions, which is analogous to selecting particular energy losses, information about the differential ionization yields were obtained. Figure 1 also shows a three-dimensional (3D) spectrum of scattered projectiles in coincidence with Ar^+ ions. Decreases in signal as a function of both scattering angle and energy loss are clearly seen.

To convert the measured coincidence signals to absolute cross sections the following procedure was used. The number of projectiles scattered into a solid angle Ω and having a final energy E that are in coincidence with the recoil ion with charge state q, $N^{q+}(\Omega,E)$, is proportional to the beam intensity N_P, the number of target atoms N_T, the solid angle, the energy range accepted ΔE, and the recoil ion detection efficiency ϵ^{q+}. Thus, the double-differential multiple-ionization cross section is given by

$$\frac{d^2\sigma^{q+}}{d\Omega dE} = \frac{N^{q+}(\Omega,E)}{\epsilon^{q+} N_P N_T \Delta\Omega \Delta E}. \tag{1}$$

Rather than measure N_P and N_T directly, we measured the number of recoils with charge state q, N_R^{q+}. These are related to the total cross sections for multiple ionization, σ^{q+}, by

$$N_R^{q+} = N_P N_T \sigma^{q+} \epsilon^{q+}. \tag{2}$$

When multiplied by the charge and summed, these partial multiple-ionization cross sections are equal to the total (gross) ionization cross sections which are available in the literature [17–21] and known to within 10%. Therefore Eq. (2) can be rewritten as

$$\sum_q q N_R^{q+} = N_P N_T \sum_q q \sigma^{q+} \epsilon^{q+}. \tag{3}$$

Equation (3) and knowledge of the gross ionization cross section were used to determine the product of the target density and the beam current and to place our data on an absolute scale.

III. RESULTS AND DISCUSSION

Using the procedures outlined, absolute double-differential cross sections (DDCSs) for single ionization of Ar by 500, 750, and 1000 eV electron impact were determined. Data for 0° are graphed in Fig. 2 as a function of the relative amount of projectile energy loss for electrons scattered into a forward cone of angles comprised around 0° in order to show projectile energy systematics. Also shown are 250 and 500 eV electron impact cross sections from DuBois and Rudd [22], which have been extrapolated to 0°. The good agreement between the present data and those from DuBois and Rudd, even at larger energy losses, demonstrates the reliability of the present apparatus and of our absolute normalization process. By scaling the projectile energy loss as was done, it is seen that as the projectile energy increases, the distribution becomes narrower and is more peaked near small energy losses due to the increasing probability of scattering at forward angles. Also, the cross sections decrease in magnitude with increasing impact energy, as expected.

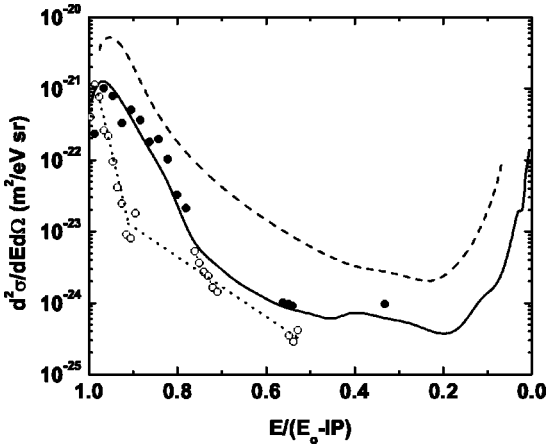

FIG. 2. Doubly differential cross sections by electron impact on argon at 0°, as a function of scaled energy of scattered projectile. E is the postcollision projectile energy, E_0 is the incoming beam energy, and IP is the ionization potential of argon. Dashed line: DDCS for 250 eV electron impact extrapolated to 0° from DuBois and Rudd [14]; solid line: same for 500 eV electron impact; closed circles: single ionization of argon by 500 eV electron impact, this work; open circles with dotted line: same for 1000 eV electron impact.

Figure 3 shows the percentage of single and multiple ionization as a function of primary energy and energy loss. In addition, the present data for electron impact are compared to our previous measurements for positron impact as well as with photoionization data from [23]. The relative yields were obtained from

$$f^{q+} = \frac{N^{q+}/\epsilon^{q+}}{\sum_j (N^{j+}/\epsilon^{j+})}, \tag{4}$$

where f^{q+} is the fraction of q times ionized argon, ϵ^{q+} is the detection efficiency for Ar^{q+}, and N^{q+} is the number of recoil ions with charge state q recorded for a particular energy loss. For 500 and 1000 eV electron impact, the angular acceptance range was $\Delta\phi = \pm 6.5°, \Delta\theta = \pm 8°$; for 750 eV electron and positron impact the ranges were $\Delta\phi = \pm 17°, \Delta\theta = \pm 17°$; for photoionization, total cross sections were used.

A. Impact energy dependence

Figure 3 shows that single target ionization dominates over the entire range of energy loss and that its contribution decreases slowly and monotonically as a function of the projectile energy loss. As was found previously for positron impact [14], the amount of double ionization increases rapidly for the first 100 eV of energy loss and then more slowly up to

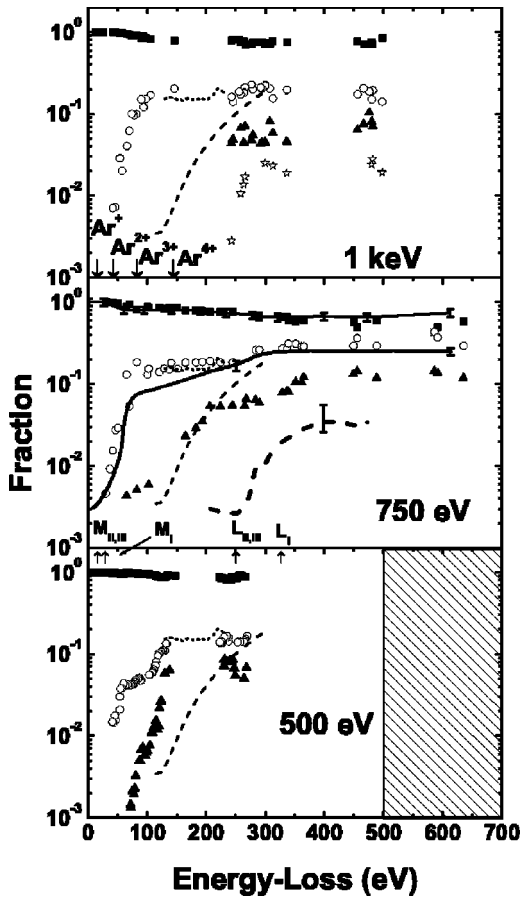

FIG. 3. Fractions of single and multiple ionization of argon as a function of the projectile energy loss for 500, 750, and 1000 eV electron impact as a function of the projectile energy loss compared with 750 eV positron impact and photoionization. Data are for different angular acceptances. See the text for details. Present data for electron impact: closed squares, single ionization; open circles, double ionization; closed triangles, triple ionization; stars, quadruple ionization. Positron impact data from Refs. [14,15]: thin solid line, single ionization; thick solid line, double ionization; thick dashed line, triple ionization. Some representative error bars have been drawn for positron impact. Photoionization from Ref. [23]: dotted lines, double ionization by photon impact; dashed lines, representative curve of triple ionization. The up arrows (top graph) indicate the appearance energies of Ar^+, Ar^{2+}, Ar^{3+}, and Ar^{4+} while the down arrows (bottom graph) indicate the binding energies. The hatched area indicates the portion of the spectra not accessible for the 500 eV electron impact.

300 eV, after which it remains constant. This is true for all impact energies investigated. A faster increase between 50 and 150 eV is observed for 1 keV and 750 eV impact than at 500 eV electron impact. In the case of triple ionization, a fast increase is seen for 500 eV impact but a much slower increase is found at 750 eV; at 1 keV no data are available near the triple-ionization threshold. At 1 keV, quadruple ionization of argon is observed only for energy losses sufficient to ionize the L shell, where after a fast increase it remains roughly constant around 2–3 %.

B. Comparisons between electron and positron impact

In the middle part of Fig. 3, positron and electron impact data are compared. Because of the lower statistics and more scatter, smooth curves have been drawn through the positron data as well as some representative error bars. No differences are observed between the single-ionization fractions resulting from electron and positron impact. But for double ionization, the relative amount of double ionization is systematically larger for electrons than for positron impact. This charge effect has been observed in total double-ionization cross sections for particle and antiparticle impact [7–9] but is now shown to be independent of energy loss (i.e., impact parameter)—at least for the forward-scattering angles investigated here. Much more noticeable is the huge enhancement observed for triple ionization by electron impact. Also, triple ionization for positron impact was not observed below 250 eV, i.e., until the L shell was ionized, whereas it is quite noticeable for electron impact. A possible explanation may be that for electron impact both the scattered projectile and the ionized target electron contribute to the energy-loss spectrum whereas for positron impact only the scattered projectile contributes.

Understanding of some of these double-ionization features can be obtained in terms of the following mechanisms [14]: the so-called shake-off process and the two-step mechanism. Shake-off is where the first electron is ejected in a direct interaction with the projectile while the second electron is ionized by the final-state rearrangement. In contrast, the two-step mechanism is where both electrons are simultaneously ejected by a direct interaction with the projectile. Another double-ionization mechanism involves ionization of an inner-shell electron followed by a postcollisional Auger decay.

Both shake-off and inner-shell ionization plus Auger decay yield a double-to-single ionization cross-section ratio that is independent of the projectile velocity. Generally, the two-step process is dominant in the intermediate-velocity regime and drops fast with the increase of the projectile velocity due to the fact that it is a second order process. But it has been suggested that this mechanism can remain significant even at high impact energies since the velocity of the first electron is rather independent of the energy of the incident particle [9].

McGuire [24] suggested that the difference in the double ionization by electrons and protons was a charge effect. That difference arises due to quantal interference between the shake-off and two-step mechanisms, giving rise to a term proportional to q^3. The distortion of the target electron wave function with respect to the presence of a positive or negative particle has also been used to explain that difference [9].

The difference in the triple ionization of gases by electron and positron impact has been also observed in the measured total cross sections and has been understood in terms of the Coulomb or trajectory effect [25]. The target nuclear repulsion experienced by the positron prohibits it from getting close to the target atom; as a consequence, the positron interacts with the target electron at larger impact parameters.

On the other hand, the projectile electron is attracted by the target nucleus and the collision takes place at smaller impact parameters, resulting in comparatively larger cross sections. This effect is more sensitive near the threshold and should decrease at higher impact velocities, in agreement with Fig. 3.

C. Comparisons between charged particle and photon impact

Charged particle data, both electron and positron, for multiple outer-shell ionization are also compared with photoionization data in Fig. 3. For 500 eV electron impact, the fractions of argon double ionization are slightly below the corresponding fractions for photoionization. At 750 eV electron impact, double-ionization fractions are slightly above those for photoionization, which are larger than those for positron impact. At 1 keV, the electron impact fractions are again larger than the photoionization fractions.

In the case of triple ionization, the present results for 500 eV electron impact are systematically higher than their corresponding values for photoionization between 100 and 150 eV but the curves cross near the $L_{\mathrm{II,III}}$ edge with the photoionization data being larger above the L edge. For 750 and 1000 eV, the relative amount of triple ionization by electron impact is smaller than for photon impact.

D. Angular distributions

Figure 4 shows the angular distributions around zero degrees for single ionization by 500 eV and 1 keV electron impact. Also shown are double-to-single ionization ratios. In both cases the angular distributions are shown for a ''small'' and a ''large'' energy loss. In order to improve statistics and due to the beam energy resolution, the data shown involve sums over 10 eV energy bins.

The angular distributions of scattered projectiles present general features, regardless of the projectile energy. For single ionization, a maximum occurs at 0°, indicating that the single ionization takes place at large impact parameters, which gives a small transverse momentum transfer to the target electron. For increasing energy loss, the intensity decreases and the distribution becomes flatter. At large energy losses, the angular distributions present a minimum around 0°, signaling that the collision takes place at small impact parameters. This broadening and appearance of a minimum at larger energy losses can be understood in terms of the binary collision between the incoming and target electrons.

The double-to-single ionization cross-section ratios are presented for small energy losses, i.e., near the double-ionization threshold (43.4 eV), and at a larger energy loss. Near the threshold of double ionization, the ratio shows a minimum at 0°, indicating that the double ionization takes place at smaller impact parameters as compared to single ionization. For increasing projectile energy loss, the ratio of double-to-single ionization is seen to be approximately constant—at least in the region around 0°.

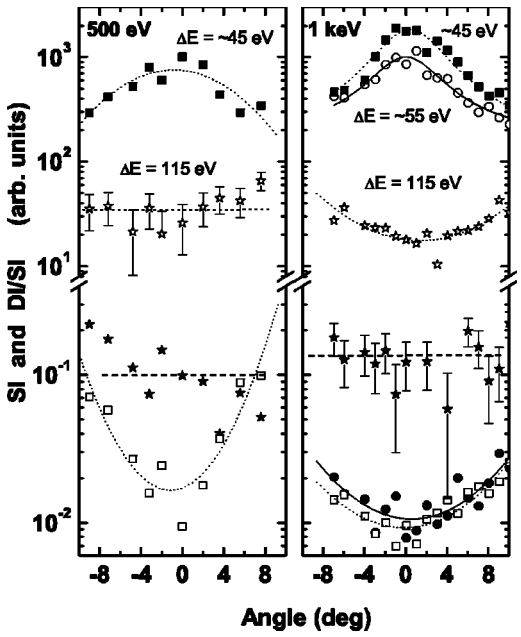

FIG. 4. Angular distributions of scattered electrons in coincidence with singly and doubly ionized argon ions for 500 eV (left figure) and 1 keV (right figure) electron impact. The angular distributions were obtained using a 10 eV energy-loss interval due to the finite energy resolution and to improve statistics. Upper portion: single ionization cross sections (arb. units); solid squares, 45 eV energy loss; open circles, 55 eV; open stars, 115 eV. Lower portion: double-to-single ionization ratios; open squares, ratios for 45 eV energy loss; solid circles, 55 eV; solid stars, 115 eV. The lines have been drawn to guide the eyes.

IV. SUMMARY AND CONCLUSIONS

In conclusion, we have measured absolute differential cross sections for single and multiple ionization of argon induced by 500, 750, and 1000 eV electron impact. Relative cross sections for single and multiple ionization of argon were determined as a function of the projectile energy loss in the range of 0–85 % of the incident projectile energy. Using these data, comparisons between particle and antiparticle impact were made at 750 eV. The fractions were also compared to those for photon impact. Finally, the angular distributions for single-ionization and double-to-single ionization cross sections were measured.

The data demonstrate that single-ionization cross sections by either electron or positron impact decrease rapidly for the first 50 eV of the projectile energy loss and then more slowly. In comparison, the double- and triple-ionization cross sections tend to decrease more slowly throughout the entire energy-loss range. Thus, the percentage of multiple ionization increases significantly with increasing energy loss. The comparison shows increasing differences between electron and positron impact cross sections as the degree of target ionization increases. These differences were explained conceptually in terms of ionization mechanisms, the change of projectile trajectory due to the attraction or repulsion of the target nucleus, and changes in binding energies of the target electrons.

ACKNOWLEDGMENTS

This work was supported by the National Science Foundation (Grant No. PHY0097902) and CNPq (Brazil).

[1] M. Inokuti, Rev. Mod. Phys. **43**, 297 (1971).
[2] W. S. Melo, A. C. F. Santos, M. M. Sant'Anna, G. M. Sigaud, and E. C. Montenegro, J. Phys. B **35**, L187 (2002).
[3] R. A. Sparrow and R. E. Olson, J. Phys. B **27**, 2647 (1994).
[4] M. Charlton and G. Laricchia, J. Phys. B **23**, 1045 (1990).
[5] G. Laricchia, in *The Physics of Electronic and Atomic Collisions*, edited by L. J. Dube, J. B. A. Mitchell, J. W. McConkey, and C. E. Brion (AIP, New York 1995), p. 385.
[6] A. Schmitt, U. Cerny, H. Möller, W. Raith, and W. Weber, Phys. Rev. A **49**, R5 (1994).
[7] Á. Kövér, G. Laricchia, and M. Charlton, J. Phys. B **26**, L575 (1993); **27**, 2409 (1994); Á. Kövér, R. M. Finch, M. Charlton, and G. Laricchia, *ibid.* **30**, L507 (1997).
[8] K. Paludan, G. Laricchia, P. Ashley, V. Kara, J. Moxon, H. Bluhme, H. Knudsen, U. Mikkelsen, S. P. Møller, E. Uggerhøj, and E. Morenzoni, J. Phys. B **30**, L581 (1997).
[9] K. Paludan, H. Bluhme, H. Knudsen, U. Mikkelsen, S. P. Møller, E. Uggerhøj, and E. Morenzoni, J. Phys. B **30**, 3951 (1997).
[10] L. H. Andersen, P. Hvelplund, H. Knudsen, S. P. Møller, A. H. Sørensen, K. Elsener, K.-G. Rensfelt, and E. Uggerhoj, Phys. Rev. A **36**, 3612 (1987).
[11] V. Kara, K. Paludan, J. Moxon, P. Ashley, and G. Laricchia, J. Phys. B **30**, 3933 (1997).
[12] H. Knudsen, L. Brun-Nielsen, M. Charlton, and M. R. Poulsen, J. Phys. B **23**, 3955 (1990).
[13] D. R. Schultz, R. E. Olson, and C. O. Reinhold, J. Phys. B **24**, 521 (1991).
[14] R. D. DuBois, C. Doudna, C. Lloyd, M. Kahveci, Kh. Khayyat, Y. Zhou, and D. H. Madison, J. Phys. B **34**, L783 (2001).
[15] R. D. DuBois, Kh. Khayyat, C. Doudna, and C. Lloyd, Nucl. Instrum. Methods Phys. Res. B **192**, 63 (2002).
[16] R. D. DuBois, Phys. Rev. A **36**, 2585 (1987).
[17] P. McCallion, M. B. Shah, and H. B. Gilbody, J. Phys. B **25**, 1061 (1992).
[18] A. Sorokin, L. A. Shmaenok, S. V. Bobashev, B. Möbus, M. Richter, and G. Ulm, Phys. Rev. A **61**, 022 723 (2000).
[19] H. C. Straub, P. Renault, B. G. Lindsay, K. A. Smith, and R. F. Stebbings, Phys. Rev. A **52**, 1115 (1995).
[20] D. P. Almeida, A. C. Fontes, I. S. Matos, and C. F. L. Godinho, J. Electron Spectrosc. Relat. Phenom. **67**, 503 (1994).
[21] D. P. Almeida, A. C. Fontes, and F. P. Pontes, Nucl. Instrum. Methods Phys. Res. B **132**, 280 (1997).
[22] R. D. DuBois and M. E. Rudd, Phys. Rev. A **17**, 843 (1978).
[23] D. M. P. Holland, K. Codling, J. B. West, and G. V. Marr, J. Phys. B **12**, 2465 (1979).
[24] J. H. McGuire, Phys. Rev. Lett. **49**, 1153 (1982).
[25] S. Helms, U. Brinkmann, J. Deiwokis, R. Hippler, H. Schneider, D. Segers, and J. Paridaens, J. Phys. B **27**, L557 (1994).